Supplement of Biogeosciences, 21, 2253–2272, 2024
https://doi.org/10.5194/bg-21-2253-2024-supplement

Biogeosciences Open Access EGU

Supplement of

Elevated atmospheric CO_2 concentration and vegetation structural changes contributed to gross primary productivity increase more than climate and forest cover changes in subtropical forests of China

Tao Chen et al.

Correspondence to: Guoping Tang (tanggp3@mail.sysu.edu.cn)

Text S1 (description of the photosynthesis module in the BEPS model)

The BEPS model was originally developed at the Canada Centre for Remote Sensing to assist in natural resources management (Liu et al., 1997). Compared with 15 prognostic models that participated in the Global Carbon Project (GCP) (Le Quere et al., 2018), BEPS results are mostly better in terms of the Pearson regression coefficient (R^2), root mean square error (RMSE), accumulated total sink, and trend against the residual land sink reported by Le Quere et al (2018). The BEPS model was mainly driven by remotely sensed datasets, which can be used for simulating the key carbon (e.g., GPP, NPP and NEP) and water (e.g., ET) fluxes of the terrestrial ecosystems at the yearly, daily and hourly scales. In the BEPS model, there are 8 plant functional types (PFTs), including shrubland, grassland, cropland, and four forest types (the evergreen needleleaf forests (ENF), deciduous needleleaf forests (DNF), deciduous broadleaf forests (DBF), evergreen broadleaf forests (EBF), mixed forests (MXF)). For the detailed structure of the BEPS model, please refer to Xing et al., (2023).

At the daily scale, the BEPS model was driven by the daily leaf area index (LAI), daily meteorological data, etc. Daily carbon fixation in the BEPS model is calculated by scaling Farquhar's leaf biochemical model (Farquhar et al., 1980) up to canopy-level implemented with a spatial and temporal scaling scheme (Chen et al., 1999). Daily gross primary productivity (GPP) is calculated separately for sunlit and shaded leaves (see Eq. (1-3) and Eq. (S1-S6)). The photosynthesis of sunlit and shaded leaves A (i.e., A_{sun} (unit: $\mu mol\ m^{-2}\ s^{-1}$) and A_{shade} (unit: $\mu mol\ m^{-2}\ s^{-1}$)) can be calculated as follows:

$$A = min\left(A_c, A_j\right) - 0.015 \times V_m \tag{S1}$$

where A_c denotes the Rubisco-limited gross photosynthesis rate ($\mu mol\ m^{-2}\ s^{-1}$) and is computed as Eq. S2; A_j is the RuBP-limited gross photosynthesis rate ($\mu mol\ m^{-2}\ s^{-1}$) and is calculated as Eq. S3.

$$A_c = V_m \frac{C_i - \Gamma}{C_i + K} \tag{S2}$$

$$A_j = J \frac{C_i - \Gamma}{4.5C_i + 10.5\Gamma} \tag{S3}$$

where C_i is the intercellular CO_2 (Pa); K is a function of enzyme kinetics (Pa) and is calculated as $K = K_C \times \left(1 + \frac{O_2}{K_O}\right)$; O_2 is oxygen concentrations in the atmosphere (Pa); K_C and K_O are the Michaelis-Menten constants for CO_2 (Pa) and O_2 (Pa), respectively; Γ denotes the CO_2 compensation point without dark respiration (Pa) and is calculated as $\Gamma = 4.04 \times 1.75^{(T_a-25)/10}$; V_{cmax} is the maximum carboxylation rate ($\mu mol\ m^{-2}\ s^{-1}$) and J represents the electron transport rate ($\mu mol\ m^{-2}\ s^{-1}$). The corresponding formulas for V_m and J are as follows:

$$V_m = V_{cmax25} \times 2.4^{\frac{T_a-25}{10}} f(T_a) f(N) \tag{S4}$$

$$f(T_a) = \left\{1 + exp\left[\frac{-220000 + 710 \times (T_a + 273)}{8.314 \times (T_a + 273)}\right]\right\}^{-1} \tag{S5}$$

$$J = (29.1 + 1.64V_m) \times PPFD / \left(PPFD + 2.1 \times (29.1 + 1.64V_m)\right) \tag{S6}$$

where V_{cmax25} is the maximum carboxylation rate at 25°C ($\mu molm^{-2}s^{-1}$); Ta is air temperature (°C); $f(N)$ is the function of nitrogen (N) and is usually set to 0.5 in the BEPS model (Liu et al., 1999; Zhang

et al., 2018), which can adjust the photosynthesis rate for foliage nitrogen (Bonan, 1995). The $PPFD$ is the photosynthesis photon flux density ($\mu mol\ m^{-2}\ s^{-1}$).

When BEPS modelled the dynamics of carbon pools beyond the GPP, it stratified soil carbon stocks into 9 pools (i.e., surface structural litter, surface metabolic litter, soil structural litter, soil metabolic litter, coarse woody litter, surface microbe, soil microbe, slow, and passive carbon pools). These 9 carbon pools were used to calculate heterotrophic respiration (R_h) and autotrophic respiration (R_a). Eventually, the net ecosystem productivity (NEP) is calculated as the difference between GPP and R_h and R_a.

$$NEP = GPP - R_h - R_a \quad \text{(S7)}$$

Table S1 Information description of flux tower sites in subtropical forest ecosystems in China.

Site name	Vegetation type	Longitude	Latitude	Time range	Reference
Ailaoshan (ALS)	Subtropical evergreen broad-leaved forest (EBF)	101.029°E	24.538°N	2009–2013	Qi et al. (2020); Yu et al. (2006)
Dinghushan (DHS)	Subtropical evergreen broad-leaved forest (EBF)	112.534°E	23.174°N	2003–2010	Yu et al. (2006)
Qianyanzhou (QYZ)	Subtropical evergreen needle-leaved forest (ENF)	115.067°E	26.733°N	2003–2010	Yu et al. (2006)

Table S2 The mean ($\pm$ standard deviation) of V_{cmax25} for different plant functional types (PFTs) calculated from the remote sensing-derived V_{cmax25} products (i.e., multi-year average) in China's subtropical forest ecosystems.

PFTs	Unit	EBF	DBF	ENF	MXF
V_{cmax25}	$\mu molm^{-2}s^{-1}$	38.55 ± 10.14	35.70 ± 6.22	38.47 ± 8.32	33.36 ± 7.96

Table S3 Details of the published GPP products were used for model comparison.

Dataset	Time Range	Spatial Resolution	Description	Source	References
MODIS GPP	2000-2022	500 m	MODIS GPP products are generated by the MOD17 algorithm and Biome-Property-Look-Up-Table by integrating the Terra/Aqua satellite observations (i.e., MODIS surface reflectances, MOD09) and meteorological data	https://ladsweb.modaps.eosdis.nasa.gov/archive/allData/6/MOD17A2H/	Running et al. (2015)
EC-LUE GPP	1982–2018	0.05°	EC-LUE GPP data are derived from the Eddy Covariance-Light Use Efficiency model by integrating several major long-term environmental variables (e.g., air temperature, leaf area index, and atmospheric water vapor pressure)	https://doi.org/10.6084/m9.figshare.8942336.v3.	Zheng et al. (2020)
NIRv GPP	1982–2018	0.05°	NIRv GPP data are generated by combining the long-term satellite observations of AVHRR reflectance from LTDR (Land Long Term Data Record v4) product and global flux sites with the machine-learning algorithm	https://doi.org/10.6084/m9.figshare.12981977.v2.	Wang et al. (2021)
VPM GPP	2000-2016	0.05°	VPM GPP products are based on an improved light use efficiency model and are driven by satellite data from MODIS (e.g., MCD12Q1, MYD11A2 and MOD09A1) and climate data from NCEP Reanalysis II	https://figshare.com/articles/dataset/Annual_GPP_at_0_5_degree/5048005	Zhang et al. (2017)
$BEPS_g$ GPP	1982–2019	0.072727°	$BEPS_g$ GPP products are generated by the process-based Boreal Ecosystem Productivity Simulator model with global calibrated parameters and are driven by remotely sensed LAI, meteorological data (e.g., CRUNCEP V8.0 dataset), soil data, etc.	http://www.nesdc.org.cn/sdo/detail?id=612f42ee7e28172cbed3d809	Chen et al. (2019); He et al. (2021)

Table S4 Comparison of simulated daily GPP vs. observed daily GPP_{EC} for all three sites in each year.

Sites	Time period	R^2	RMSE (g C m^{-2} day^{-1})	MBE (g C m^{-2} day^{-1})
ALS	2009	0.50	1.69	-0.01
	2010	0.72	1.56	-0.10
	2011	0.66	1.49	-0.11
	2012	0.53	1.50	-0.14
	2013	0.53	1.57	0.17
	Overall	0.58	1.57	-0.04
DHS	2003	0.44	1.09	0.38
	2004	0.58	0.95	-0.01
	2005	0.65	1.24	0.88
	2006	0.49	1.21	0.44
	2007	0.47	1.16	0.01
	2008	0.43	1.20	-0.22
	2009	0.43	1.21	0.48
	2010	0.49	1.05	0.01
	Overall	0.44	1.17	0.24
QYZ	2003	0.77	1.27	-0.40
	2004	0.85	1.12	0.18
	2005	0.84	1.06	0.03
	2006	0.78	1.42	-0.00
	2007	0.71	1.46	-0.62
	2008	0.79	1.34	-0.38
	2009	0.76	1.40	-0.40
	2010	0.70	1.60	-0.64
	Overall	0.77	1.36	-0.29

Table S5 Comparison of simulated daily NEP vs. observed daily NEP for all three sites in each year.

Sites	Time period	R^2	RMSE (g C m^{-2} day^{-1})	MBE (g C m^{-2} day^{-1})
ALS	2009	0.21	1.69	0.01
	2010	0.20	1.54	0.04
	2011	0.21	1.49	-0.07
	2012	0.37	1.21	-0.10
	2013	0.24	1.29	0.27
	Overall	0.25	1.46	0.02
DHS	2003	0.41	1.08	0.37
	2004	0.45	0.95	-0.01
	2005	0.42	1.25	0.86
	2006	0.38	1.21	0.42
	2007	0.26	1.16	-0.01
	2008	0.26	1.20	-0.18
	2009	0.49	1.21	0.54
	2010	0.38	1.05	0.01
	Overall	0.35	1.14	0.24
QYZ	2003	0.33	1.27	0.04
	2004	0.57	1.12	0.17
	2005	0.54	1.06	0.03
	2006	0.48	1.42	0.07
	2007	0.36	1.46	-0.04
	2008	0.46	1.31	0.12
	2009	0.36	1.40	0.04
	2010	0.27	1.60	-0.09
	Overall	0.42	1.34	0.04

Table S6 Sites information of the measured net primary productivity (NPP) data used in this study

ID	Longitude	Latitude	Measured NPP (g C/m^2/year)	References
1	112.53	23.17	395.95	Yang et al., 2017
2	101.02	24.53	976.15	Tan et al., 2011
3	115.05	26.73	487.51	Yang et al., 2017
4	109.75	26.83	313.40	Zhang, 2010
5	112.86	29.53	515.65	Han, 2008
6	116.99	30.47	506.10	Han, 2008
7	113.91	33.35	343.40	Geng, 2011
8	109.445	28.405	640.15	Fan et al., 2011,
9	109.445	28.405	591.25	Fang et al., 2003
10	109.445	28.405	742.39	Fang et al., 2002
11	110.515	27.505	484.55	Lan et al., 2004
12	106.985	26.455	626.81	Li et al., 2007
13	106.985	26.455	471.22	Li et al., 2008
14	106.985	26.455	493.45	Liang et al., 2007
15	106.985	26.455	626.81	Liu et al., 2007
16	106.985	26.455	529.01	Liu et al., 2007
17	109.675	23.755	382.31	Luo et al., 2011
18	109.675	23.755	426.76	Luo et al., 2011
19	109.785	26.915	222.27	Luo et al., 2011
20	108.355	22.975	448.99	Qi et al., 2007
21	109.835	22.625	1138.04	Qin et al., 2011
22	100.855	23.205	1200.27	Xia et al., 2010
23	100.855	23.205	1066.90	Xia et al., 2010
24	99.455	24.335	1089.14	Xia et al., 2010
25	99.455	24.335	817.96	Xiong et al., 2006
26	107.965	25.305	635.70	Yang et al., 2008
27	107.955	25.305	569.02	Yang et al., 2001
28	111.885	23.455	764.62	Yang et al., 2003
29	111.885	23.455	831.30	Yang et al., 2003
30	108.355	22.975	422.32	Ye et al., 2010
31	108.355	22.975	711.27	Ye et al., 2010
32	108.355	22.975	733.50	Ye et al., 2010
33	112.535	23.175	915.76	Yin et al., 2010

Table S7 Land-cover change transition matrix for the 2001–2018 period in the subtropical region of China. EBF: evergreen needle-leaved forest; DBF: deciduous broad-leaved forest; ENF: evergreen needle-leaved forest; MF: mixed forest; CRO: cropland; GRA: grassland; SHR: shrubland; URB: urban; and BAR: bare land. Green and red arrows indicate a net increase and a net decrease, respectively.

		2018 ($\times10^3$ km^2)										
		EBF	**DBF**	**ENF**	**MXF**	**CRO**	**GRA**	**SHR**	**URB**	**BAR**	**Total**	**Losses**
2001 ($\times10^3$ km^2)	**EBF**	551.08	0.38	1.72	7.79	3.03	0.13	0.42	0.00	0.10	564.66	13.57
	DBF	0.64	89.62	0.16	2.97	0.26	0.03	0.03	0.03	0.00	93.74	4.12
	ENF	3.48	0.06	492.41	19.04	13.10	0.80	0.32	0.29	0.03	529.52	37.11
	MXF	8.50	1.12	10.73	275.61	3.00	0.48	0.13	1.72	0.16	301.44	25.84
	CRO	12.33	2.14	4.18	4.63	1089.49	0.80	0.64	34.75	1.53	1150.49	61.00
	GRA	0.29	0.10	1.57	1.98	0.67	127.85	0.00	4.95	0.10	137.50	9.65
	SHR	5.59	0.67	2.17	1.02	3.39	0.10	9.58	0.22	0.10	22.84	13.25
	URB	0.00	0.00	0.00	0.00	0.03	0.00	0.00	23.76	0.00	23.79	0.03
	BAR	0.10	0.03	0.00	0.06	0.67	0.10	0.83	0.93	56.18	58.90	2.71
	Total	582.00	94.13	512.95	313.10	1113.63	130.28	11.95	66.66	58.19	–	–
	Gains	30.92	4.50	20.54	37.50	24.15	2.43	2.36	42.89	2.01	–	–
	Net changes	**17.34↑**	**0.38↑**	**-16.58↓**	**11.66↑**	**-36.86↓**	**-7.22↓**	**-10.89↓**	**42.86↑**	**-0.70↓**	–	–

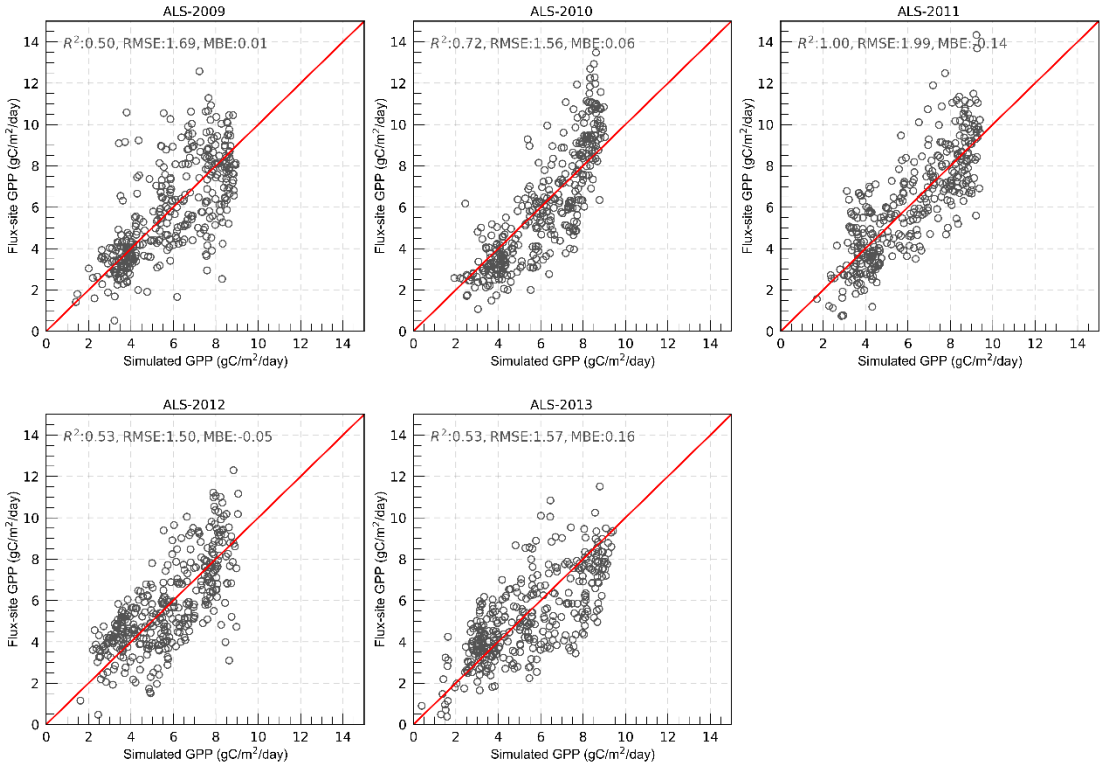

Figure S1 Scatter plots show the year-to-year (2009-2013) comparison between the simulated and observed daily GPP in the Ailao Shan flux tower station (ALS). The red line denotes the 1:1 line.

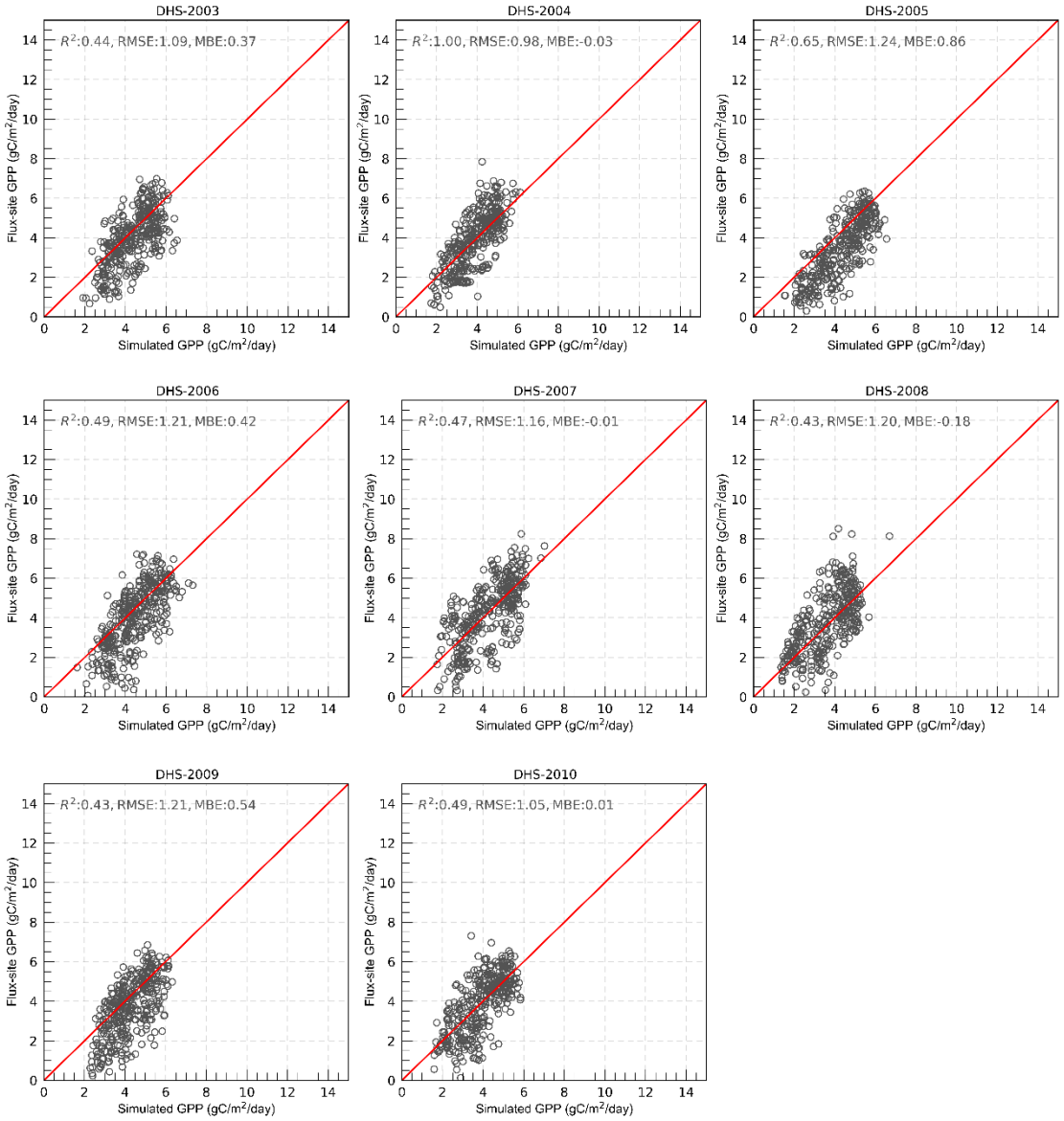

Figure S2 Scatter plots show the year-to-year (2003-2010) comparison between the daily simulated GPP with observed GPP in Dinghu Shan flux tower station (DHS).

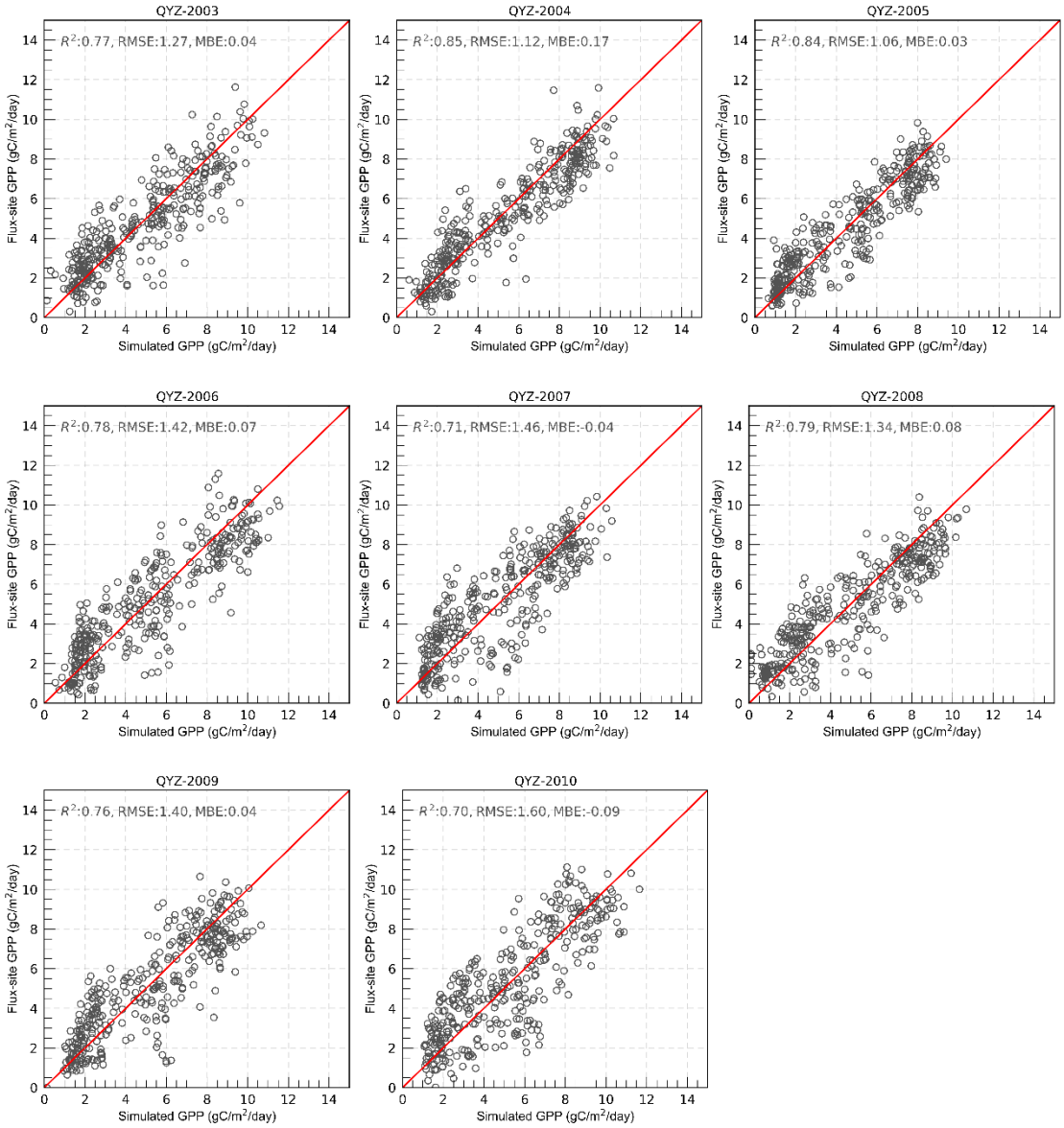

Figure S3 Scatter plots show the year-to-year (2003-2010) comparison between the daily simulated GPP with observed GPP in Qianyan Zhou flux tower station (QYZ).

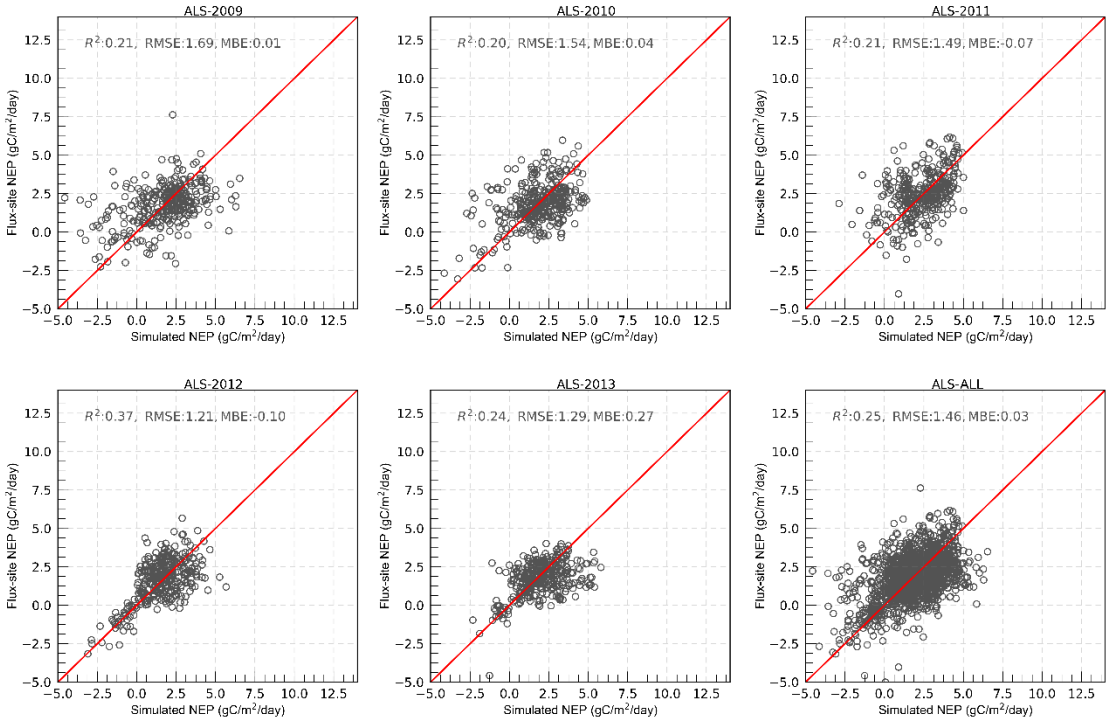

Figure S4 Scatter plots show the year-to-year (2009-2013) comparison between the daily simulated NEP with observed NEP in the Ailao Shan flux tower station (ALS). The red line denotes the 1:1 line.

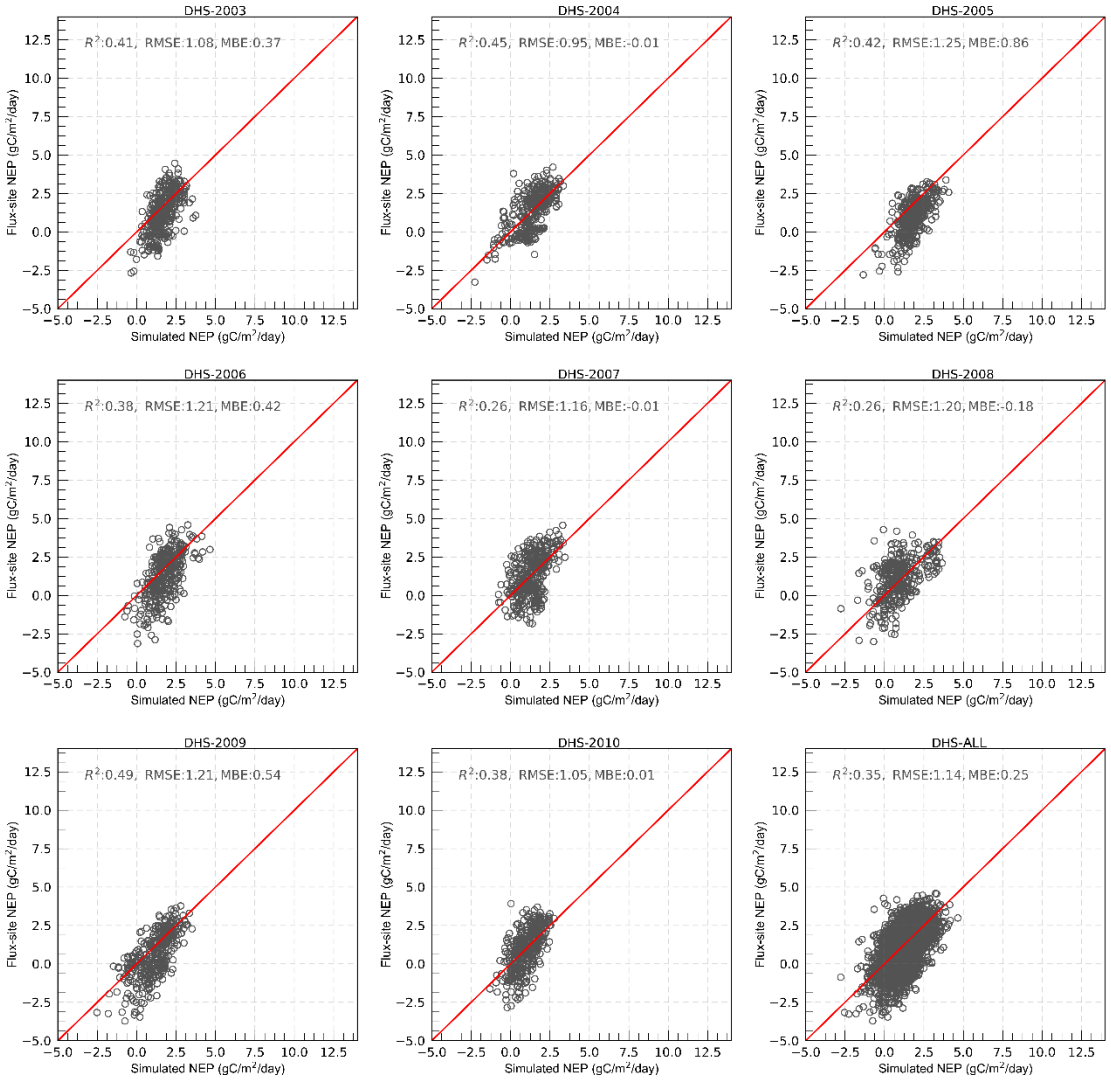

Figure S5 Scatter plots show the year-to-year (2003-2010) comparison between the daily simulated NEP with observed NEP in Dinghu Shan flux tower station (DHS). The red line denotes the 1:1 line.

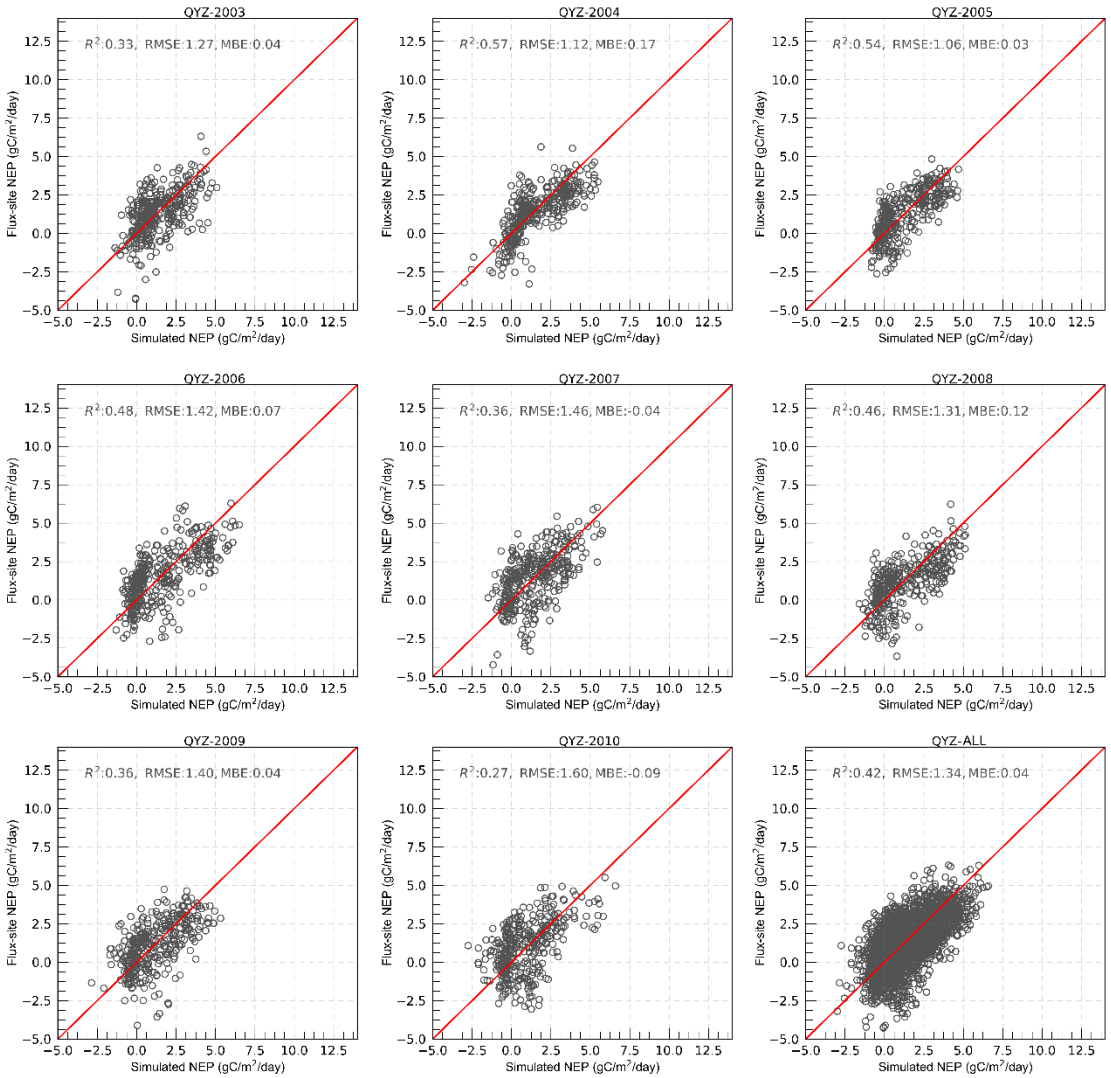

245 **Figure S6** Scatter plots show the year-to-year (2003-2010) comparison between the daily simulated NEP with observed NEP in Qianyan Zhou flux tower station (QYZ). The red line denotes the 1:1 line.

250

255

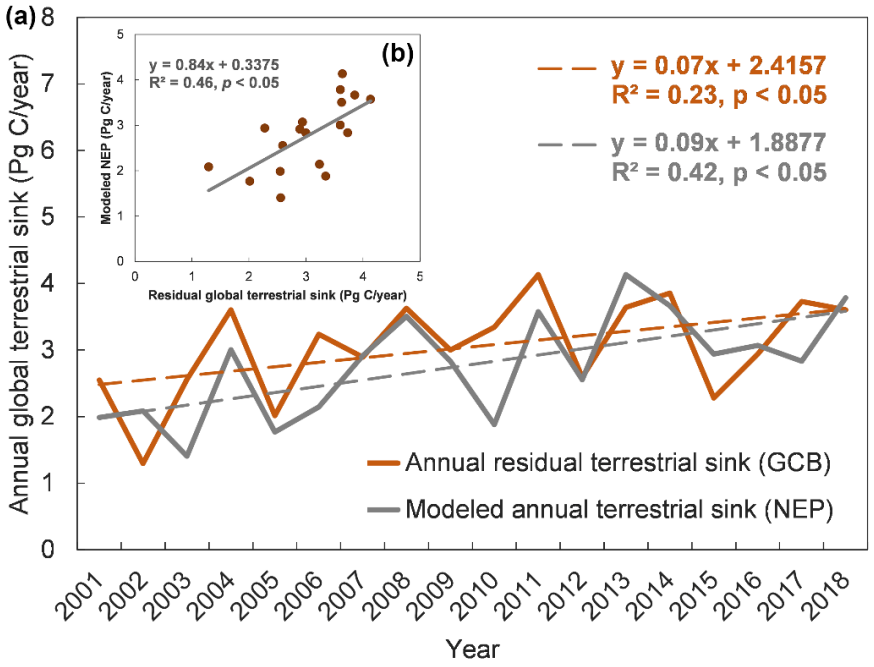

Figure S7 Comparison of the simulated annual terrestrial sink (NEP) by BEPS model and the residual terrestrial sink estimated by the Global Carbon Project (a). The insert figure represents the correlation between the simulated annual terrestrial sink (NEP) by BEPS model and annual residual terrestrial sink estimated by the Global Carbon Project (b). Here, we obtained the annual terrestrial sink from Global Carbon Budget 2023 provided by the Global Carbon Project (Friedlingstein et al., 2023), and used it for comparison. The annual terrestrial sink is computed as the sum of emissions from fossil fuel consumption, cement production, and land-use change minus the sum of CO_2 accumulated each year in the atmosphere and ocean (i.e., the annual global residual terrestrial sink). Considering that GCB only provides annual global terrestrial CO_2 sink data, we also re-simulated annual global NEP based on BEPS model to make it comparable.

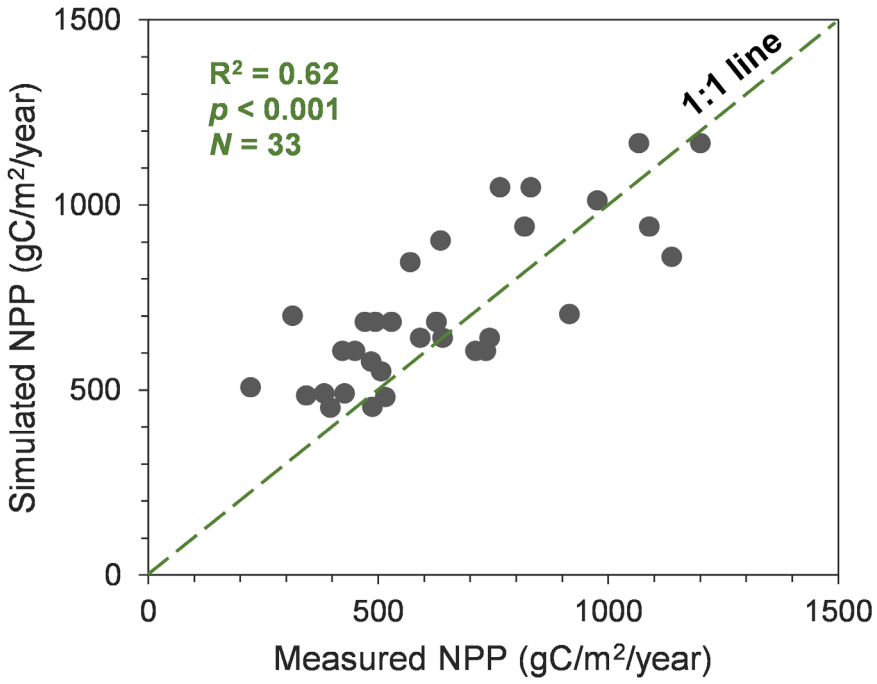

Figure S8 Validation of modelled forest NPP using measured forest NPP in the Chinese subtropics

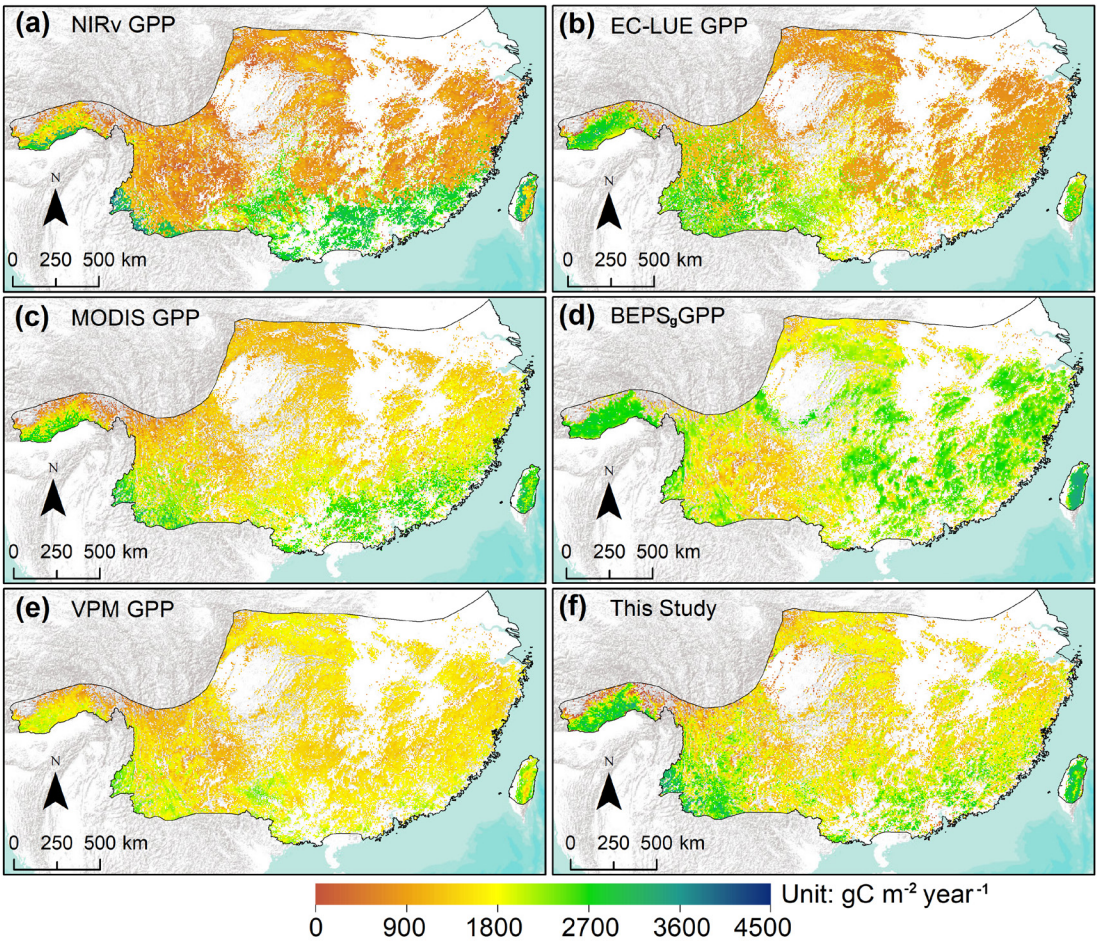

Figure S9 Comparison of the spatial distribution of the mean annual GPP. (a) NIRv GPP, (b) EC-LUE GPP, (c) MODIS GPP, (d) another published BEPS GPP (i. e., BEPS$_g$ GPP), and (f) our simulated GPP. All the maps were calculated over the 2001–2018 period, except for VPM GPP which is only available from 2001 to 2016.

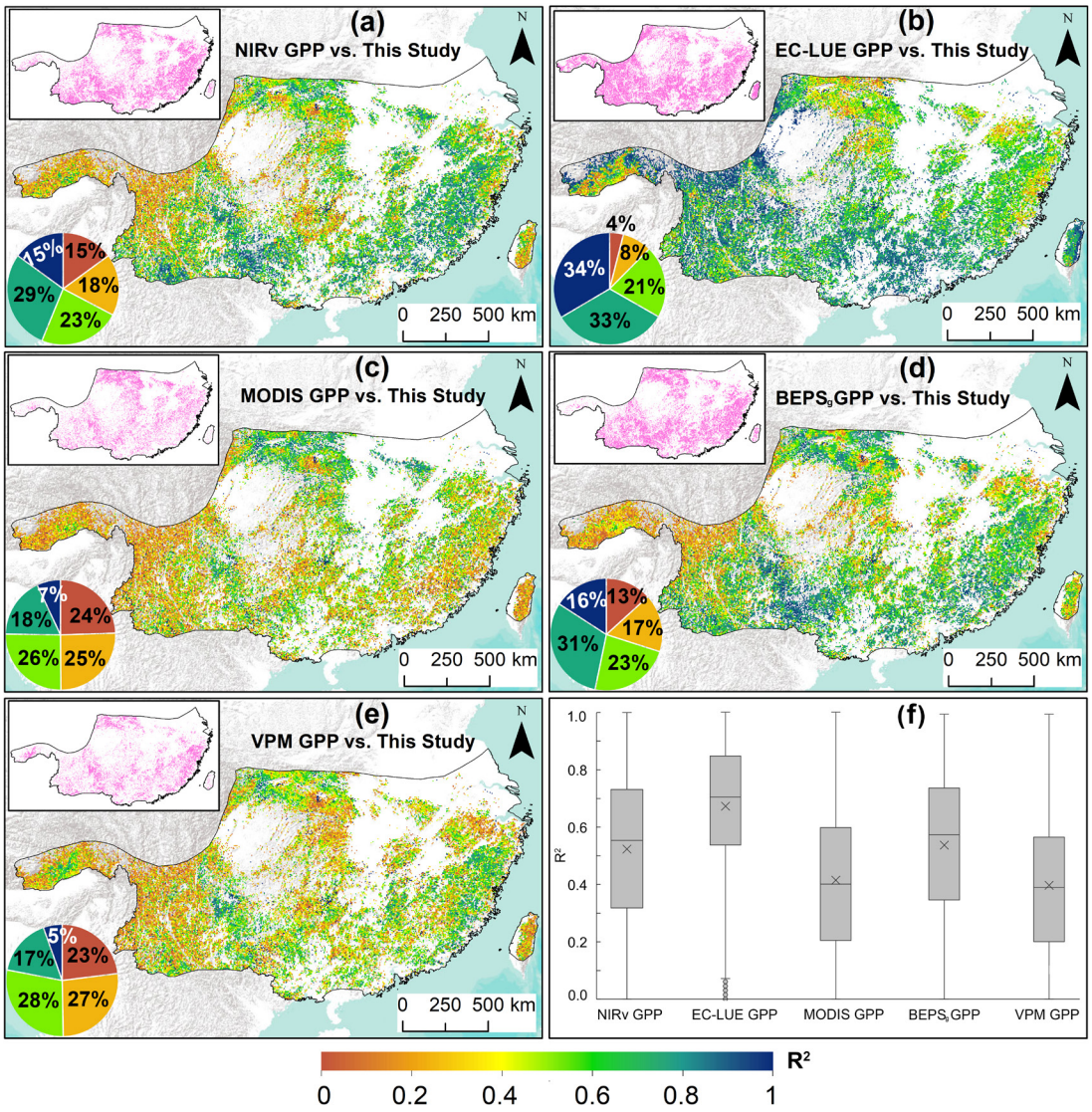

Figure S10 Spatial distribution of the determination coefficient (R^2) between our simulated GPP and five GPP products at annual scale (a-e). The insert pie charts represent the ratios of different R^2, which corresponds to the color bar. (f) Box chart is statistical results of R^2 between our simulated GPP and five GPP products. The black horizontal line in the boxplot is the median, and the cross represents the mean. Insets in (a-e) represent the subset of pixels where our simulated GPP is significantly correlated with the five GPP products at the $P < 0.05$ confidence level.

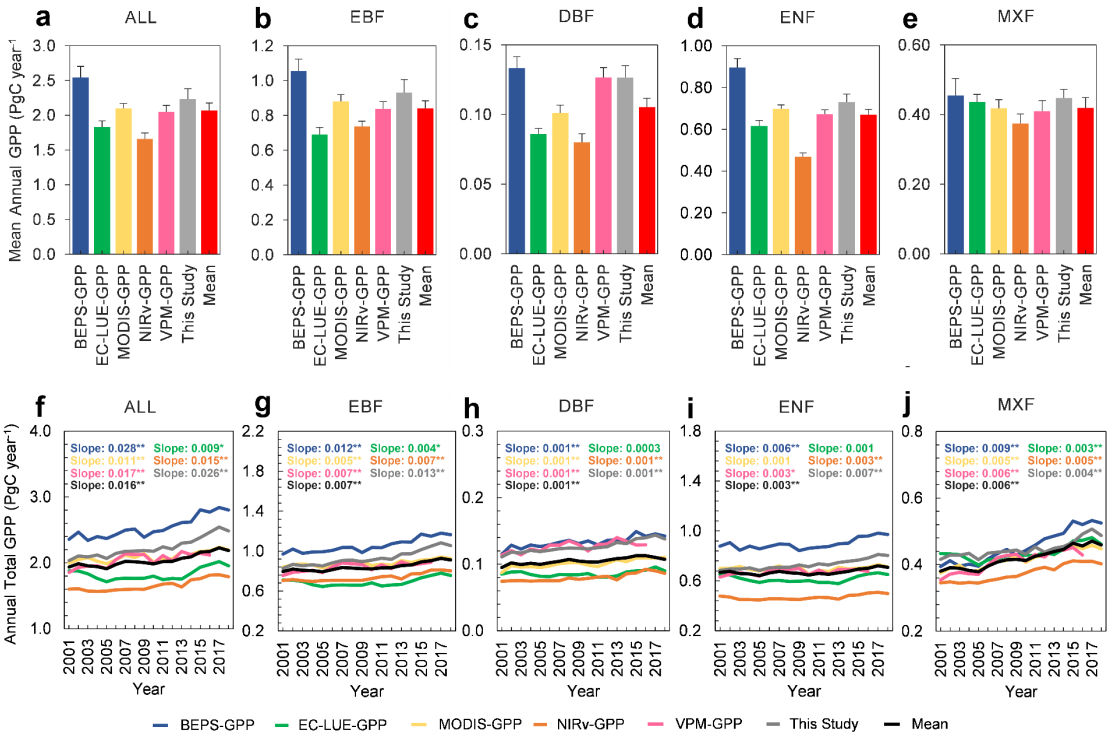

Figure S11 Comparison of the multi-year mean of annual total GPP (a-e) and the annual GPP trends (f-g) between our simulated GPP and other five published GPP products for the entire study area and different forest types. The VPM GPP can be available from 2001 to 2016 and thus the multi-year mean of annual VPM is calculated from the period 2001-2016. The grey bar in (a-e) is the standard deviation (SD). The mean denotes the average of five products. EBF: evergreen needleleaf forest; DBF: deciduous broadleaf forest; ENF: evergreen needleleaf forest; MF: mixed forest.

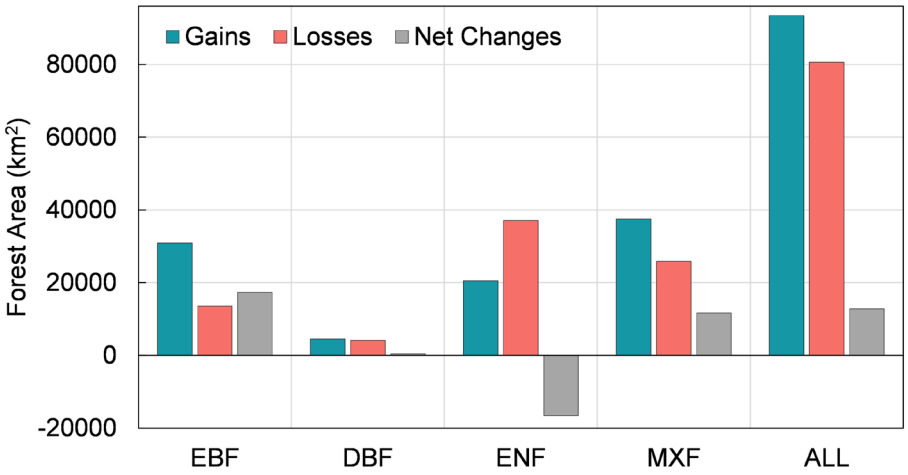

Figure S12 Changes in forest areas between 2001 and 2018.

340

345

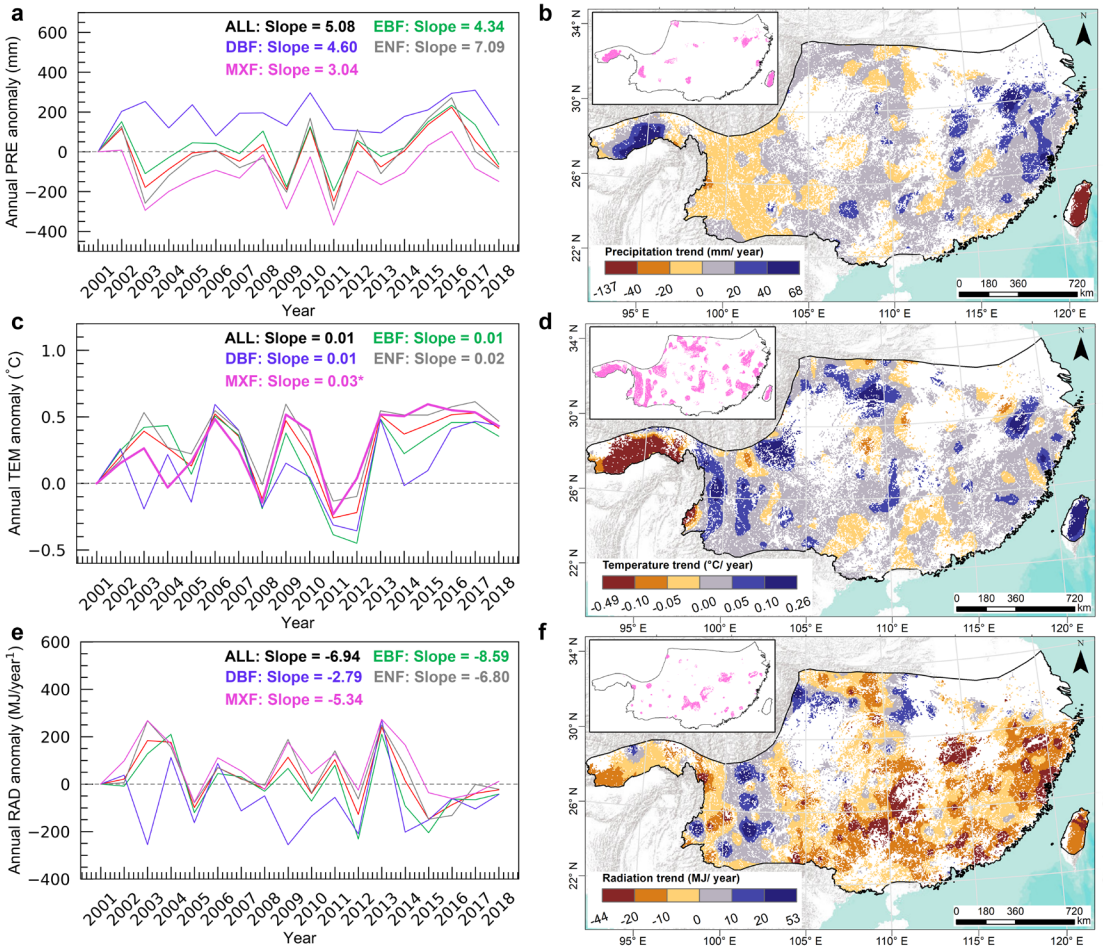

Figure S13 Annual variations of the major climate variables on the entire forest area and different forest areas from 2001 to 2018. The left column is the temporal changes of annual total precipitation anomaly (a), annual mean temperature anomaly (c), and annual total radiation anomaly (e), respectively. The right column is the spatial distribution of annual total precipitation trends (b), annual mean temperature trends (d), and annual total radiation trends (f), respectively. The anomalies are all relative to the base year 2001. Insets in (b), (d), and (f) denote the subset of pixels with significant annual precipitation, temperature, and radiation changes at $P < 0.05$. White in the study area indicates non-forested areas. EBF: evergreen needleleaf forest; DBF: deciduous broadleaf forest; ENF: evergreen needleleaf forest; MF: mixed forest.

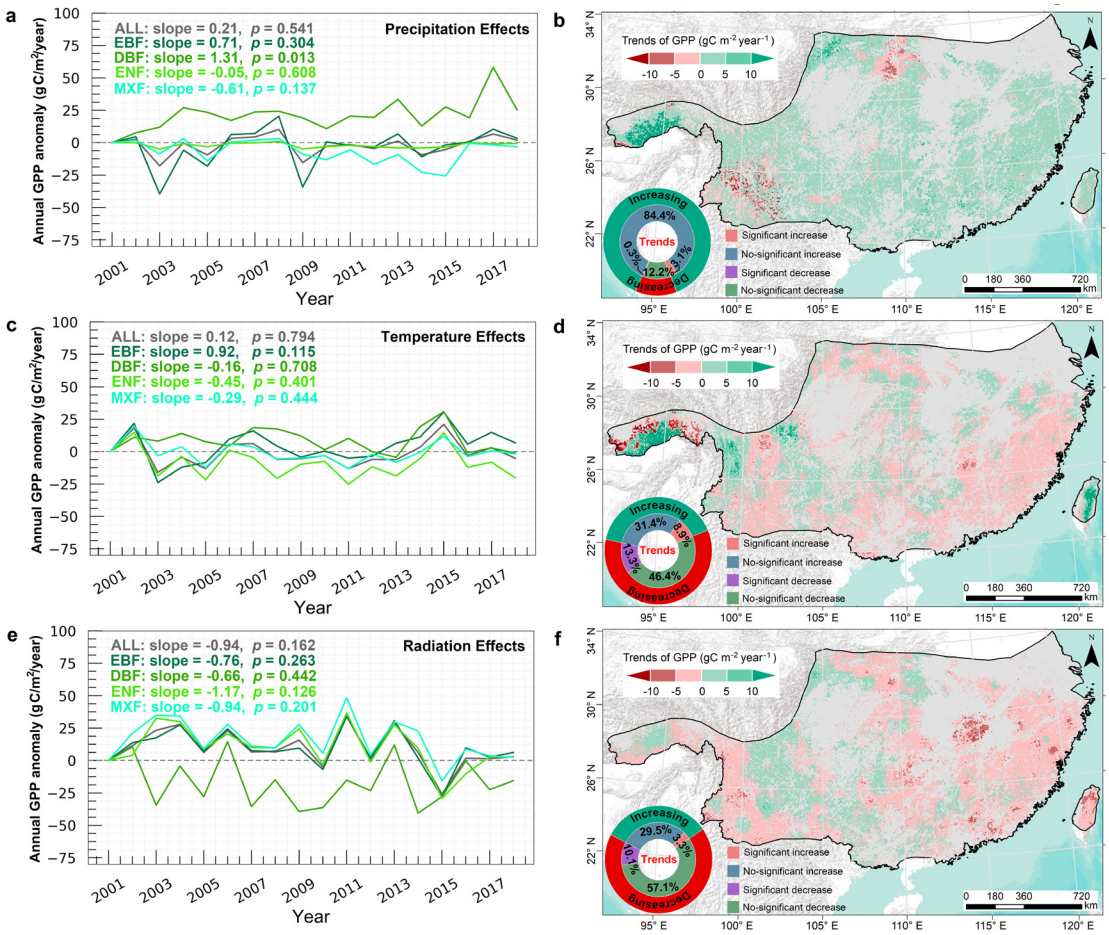

Figure S14 Temporal variation of the effects of precipitation (a), temperature (c), solar radiation (e), and all climate changes (g) on annual GPP trends. Spatial distribution of the impacts of precipitation (b), temperature (d), solar radiation (f), and all climate changes (h) on subtropical forest GPP. Grey in the study area (i.e., b, d, f, and h) indicates non-forested areas.

Description of Figure S14: Simulation results showed that an increase in precipitation induced the GPP enhancement at the rate of 0.21 gC/m^2/year (p = 0.541) for all the forest types together (Fig. S14a). The negative effect of precipitation on ENF GPP (-0.05 gC/m^2/year, p = 0.608) and MXF GPP (-0.61 gC/m^2/year, p = 0.137) was mainly offset by EBF GPP (0.71 gC/m^2/year, p = 0.304) and DBF GPP (1.31 gC/m^2/year, p = 0.013) enhancements (Fig. S14a). Spatially, the positive effect of precipitation on GPP changes accounted for most parts of the total area (87.5%), of which 3.1% showed a significant (p < 0.05) increase, mainly located in the west and north, which was consistent with the trends in the spatial distribution of precipitation (Fig. S14b). Precipitation also caused a small part of GPP (12.5%) decrease, and there is almost no significant decrease trend (Fig. S14b). Changes in temperature slightly increased the GPP across all forest types (Fig. S14c), but it showed great spatial variations (Fig. S14d). The significantly negative effect of temperature on GPP (13.3%) was mainly distributed in the south and west, while the significantly positive effect of temperature on GPP (8.9%) was mainly located in the western mountainous areas (Fig. S14d). Decreasing solar radiation (Fig. S14e) led to the negative impact of all the forest area (-0.94 gC/m^2/year, p = 0.162) as well as different forest types (EBF: -0.76 gC/m^2/year, p = 0.263; DBF: -0.66 gC/m^2/year, p = 0.442; ENF: -1.17 gC/m^2/year, p = 0.126; MXF: -0.94 gC/m^2/year,

$p = 0.201$). The decrease in solar radiation caused a significant decrease in GPP of 10.1% ($p < 0.05$) (Fig. S14f). A small portion of the study areas exhibited GPP enhancement under the influence of solar radiation, but it was hardly significant (3.3%).

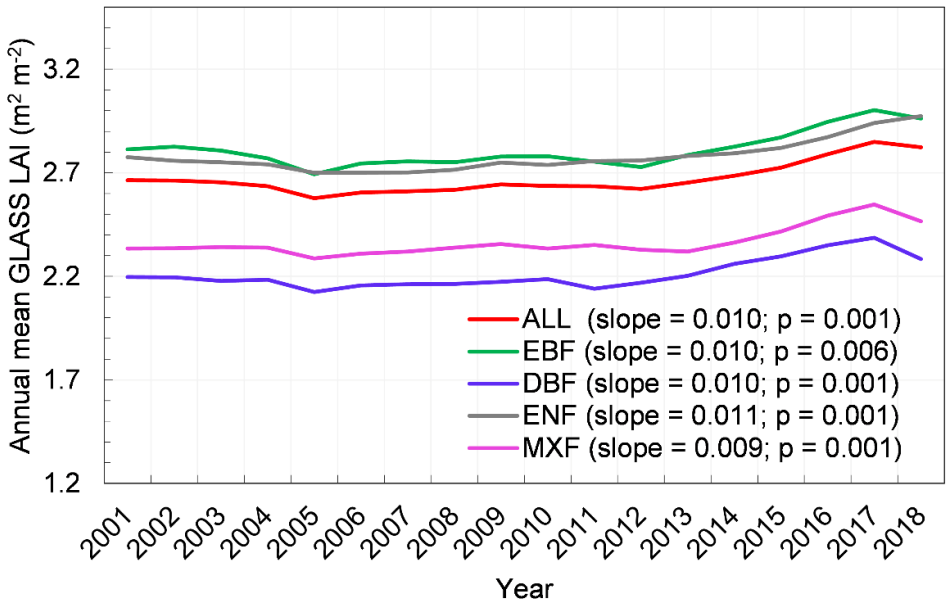

Figure S15 Annual changes of GLASS LAI for entire forest region and different forest types. EBF: evergreen needleleaf forest; DBF: deciduous broadleaf forest; ENF: evergreen needleleaf forest; MF: mixed forest.

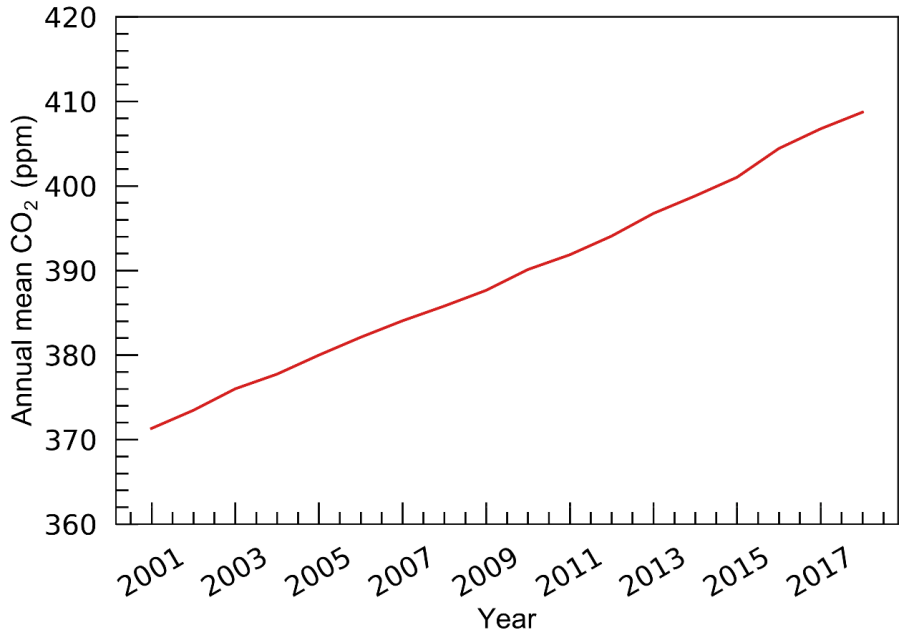

Figure S16 Temporal changes of annual mean CO_2 concentration from 2001 to 2018.

References

Bonan, G.B., 1995. Land-atmosphere CO2 exchange simulated by a land surface process model coupled to an atmospheric general circulation model Journal of Geophysical Research, 100(D2): 2817-2831.

Chen, J.M., et al., 1999. Daily canopy photosynthesis model through temporal and spatial scaling for remote sensing applications. Ecological Modelling, 124, 99-119.

Chen, J.M., Ju, W., Ciais, P., Viovy, N. and Lu, X., 2019. Vegetation structural change since 1981 significantly enhanced the terrestrial carbon sink. Nature Communications, 10(1): 4259.

Fan, J.Y. et al., 2011. Research on the tree biomass and productivity of Cryptomeria fortunei Hooibrenk plantation. Journal of Fujian Forestry Science and Technology, 38, 1–5.

Fang, X. et al., 2003. Productivity and carbon dynamics of Masson Pine plantation. Journal of Central South Forestry University, 23, 11–15.

Fang, Y.T. and Mo, J.M. 2002. Study on carbon distribution and storage of a pine forest ecosystem in Dinghushan Biosphere Reserve. Guihaia, 22, 305–310.

Farquhar, G.D., et al., 1980. A biochemical-model of photosynthetic CO_2 assimilation in leaves of C-3 Species. Planta, 149, 78-90.

Friedlingstein, P., et al., 2023. Global Carbon Budget 2023. Earth System Science Data, 15, 5301–5369.

Han, S., 2008. Productivity estimation of the poplar plantations on the beaches in middle and low reaches of Yangtze river using eddy covariance measurement. Unpublished Master Chinese Academy of Forestry, Beijing, P.R. China (in Chinese with English abstract), 75 pp.

He, Q. et al., 2021. Drought Risk of Global Terrestrial Gross Primary Productivity Over the Last 40 Years Detected by a Remote Sensing-Driven Process Model. Journal of Geophysical Research: Biogeosciences, 126(6): e2020JG005944.

Geng, S., 2011. Study on the carbon flux observation over poplar plantation ecosystem of XiPing city in Henan Province of China. Unpublished Master Beijing Forestry University, Beijing, P.R.China (in Chinese with English abstract), 91 pp.

Lan, Z.J. et al., 2004. Biomass distribution of major plant communities in Jiuzhaigou valley, Sichuan. Chinese Journal of Appplied Environmental Biology, 10, 299–306.

Le Quere, C., 2018. Global carbon budget 2017. Earth System Science Data, 10, 405-448.

Li, W.B., et al., 2007. Biomass compositions of Pinus tabulaeformis plantation and their relationships in the Dagou valley of the upper Minjiang River. Journal of Mountain Science, 25, 236–244.

Li, Z.H. et al., 2008. Effects of stand density upon the biomass and productivity of Eucalyptus urograndis. Journal of Central South Forestry University, 28, 49–54.

Liang, N. et al., 2007. A study on biomass in sapling stage of pure Betula alnoides forest and Betula alnoides and Cinnamomum cassia mixed forest. Journal of West China Forestry

Science, 36, 44–49.

Liu, J., et al., 1997. A process-based boreal ecosystem productivity simulator using remote sensing inputs. Remote Sensing Environment, 62, 158-175.

Liu, J., Chen, J.M., Cihlar, J. and Chen, W., 1999. Net primary productivity distribution in the BOREAS region from a process model using satellite and surface data. Journal of Geophysical Research: Atmospheres, 104(D22): 27735-27754.

Liu, X.C., et al., 2007. Biomass study of the plantation of Alnus cremastogyne Burkill at different stages of age. Journal of Central South Forestry University, 27, 83–86.

Luo, J. et al., 2011. Study on biomass of different types for protection forest system area around Dongting Lake. Hunan Forestry Science and Technology, 38, 27–29.

Qi, D. et al., 2020. A dataset of carbon and water fluxes observation in subtropical evergreen broad-leaved forest in Ailao Shan from 2009 to 2013. China Scientific Data, 6(1). (2021-03-06) DOI: 10.11922/sciencedb.00186.

Qi, L.H. et al., 2007. Species diversity and biomass allocation of vegetation restoration communities on degraded lands. Chinese Journal of Ecology, 26, 1697–1702.

Qin, W.M., et al., 2011. Study on the biomass and growth law of Paramichelia baillonii plantation. Journal of Fujian College of Forestry, 31, 110–114.

Running, S.W., Mu, Q. and Zhao, M., 2015. MOD17A2H MODIS/Terra Gross Primary Productivity 8-Day L4 Global 500m SIN Grid. NASA LP DAAC. http://doi.org/10.5067/MODIS/MOD17A2H.006.

Tan ZH, et al., 201. An old-growth subtropical Asian evergreen forest as a large carbon sink. Atmospheric Environment, 45, 1548-1554.

Wang, S., et al., 2021. Tracking the seasonal and inter-annual variations of global gross primary production during last four decades using satellite near-infrared reflectance data. Science of the Total Environment, 755(Pt 2): 142569.

Xia, H.B. 2010. Biomass and net primary production in different successional stages of karst vegetation in Maolan, SW China. Guizhou Forestry Science and Technology, 38, 1–7.

Xing et al., 2023. Modeling China's terrestrial ecosystem gross primary productivity with BEPS model: Parameter sensitivity analysis and model calibration. Agricultural and Forest Meteorology, 343, 15, 109789.

Xiong, D.G. et al., 2006. A study of annual growth and biomass of Alnus formosana in Yuanba District of Guangyuan City. J. Sichuan Forestry Science and Technology, 27, 55–58.

Yang, L.L. et al., 2008. Comparison between biomass and productivity of young Alnus cremastogyne Burkill plantation under different site conditions. Journal of Central South University of Forestry & Technology, 28, 122–126.

Yang, J. et al., 2017. Nonlinear Variations of Net Primary Productivity and Its Relationship with Climate and Vegetation Phenology, China. Forests, 8, 361.

Yang, Q.P. et al., 2001. Studies on the dynamic succession of Pinus massoniana community in

Heishiding Natural Reserve. Guihaia, 21, 295–300.

Ye, S.M.; Wen, Y.G.; Yang, M.; Liang, H.W.; Lan, J.X. Correlation analysis on productivity and plant diversity of Eucalyptus plantations under successive rotation. Acta Bot. Boreal.-Occident. Sin. 2010, 30, 1458–1467.

Yin, G.Q. et al., 2010. Studies on biomass of different young forests converted from farm land in Huitong, Hunan Province. Journal of Central South University of Forestry & Technology, 30, 9–14.

Yu, G.-R. et al., 2006. Overview of ChinaFLUX and evaluation of its eddy covariance measurement. Agricultural and Forest Meteorology, 137(3-4): 125-137.

Zhang LP, 2010. Characteristics of CO2 flux in a Chinese Fir Plantations Eeosystem in Huitong County,Hunan Province. Unpublished Master Central South University of Forestry and Technology,Changsha, P.R.China (in Chinese with English abstract), 61 pp.

Zhang, Y. et al., 2017. A global moderate resolution dataset of gross primary production of vegetation for 2000-2016. Scientific Data, 4: 170165.

Zheng, Y. et al., 2020. Improved estimate of global gross primary production for reproducing its long-term variation, 1982–2017. Earth System Science Data, 12(4): 2725-2746.

Zhang, S. et al., 2018. Evaluation and improvement of the daily boreal ecosystem productivity simulator in simulating gross primary productivity at 41 flux sites across Europe. Ecological Modelling, 368: 205-232.